SCIENCE CHINA
Physics, Mechanics & Astronomy

• Article •

November 2014 Vol. 57 No. 11: 2152–2160
doi: 10.1007/s11433-014-5586-y

Molecular kinetic theory of boundary slip on textured surfaces by molecular dynamics simulations†

WANG LiYa[1], WANG FengChao[1*], YANG FuQian[2] & WU HengAn[1*]

[1] *CAS Key Laboratory of Mechanical Behavior and Design of Materials, Department of Modern Mechanics, University of Science and Technology of China, Hefei 230027, China;*

[2] *Materials Program, Department of Chemical and Materials Engineering, University of Kentucky, Lexington 40506, USA*

Received July 15, 2014; accepted August 11, 2014; published online August 29, 2014

A theoretical model extended from the Frenkel-Eyring molecular kinetic theory (MKT) was applied to describe the boundary slip on textured surfaces. The concept of the equivalent depth of potential well was adopted to characterize the solid-liquid interactions on the textured surfaces. The slip behaviors on both chemically and topographically textured surfaces were investigated using molecular dynamics (MD) simulations. The extended MKT slip model is validated by our MD simulations under various situations, by constructing different complex surfaces and varying the surface wettability as well as the shear stress exerted on the liquid. This slip model can provide more comprehensive understanding of the liquid flow on atomic scale by considering the influence of the solid-liquid interactions and the applied shear stress on the nano-flow. Moreover, the slip velocity shear-rate dependence can be predicted using this slip model, since the nonlinear increase of the slip velocity under high shear stress can be approximated by a hyperbolic sine function.

textured surfaces, boundary slip, molecular dynamics simulations, molecular kinetic theory

PACS number(s): 68.08.-p, 83.50.Rp, 47.61.-k, 61.20.Ja

Citation: Wang L Y, Wang F C, Yang F Q, et al. Molecular kinetic theory of boundary slip on textured surfaces by molecular dynamics simulations. Sci China-Phys Mech Astron, 2014, 57: 2152–2160, doi: 10.1007/s11433-014-5586-y

1 Introduction

Modeling fluid flows over a textured surface have attracted increasing attention especially over the past decade [1]. The super-hydrophobic lotus leaves capable of self-cleaning [2] and the shark skin with the ability of drag reduction [3,4] are two excellent examples from nature. To utilize these phenomena in the practical applications such as molecular switches and biosensors [5,6], it is essential to understand the underlying mechanisms of boundary slip on textured surfaces [7,8].

In recent years, boundary slip on textured surfaces has been investigated intensely, both by experiments [9–11] and molecular dynamics (MD) simulations [12–18]. The boundary slip is affected by many factors, such as surface wettability [19,20], surface roughness [16,21], applied shear stress [22,23], viscosity changes near interface [24] and the presence of chemical functionalization [25]. Besides, slip is also determined by the interfacial liquid molecules distribution, which becomes more prominent in textured surfaces [26]. When we consider the onset of the slip, it is generally accepted that the slip occurs only when the applied shear stress is larger than a critical value, which is termed as the critical shear stress [27]. Our previous work has confirmed that the critical shear stress increases exponentially with the liquid-solid interactions [27]. There are some existing slip

*Corresponding author (WU HengAn, email: wuha@ustc.edu.cn; WANG FengChao, email: wangfc@ustc.edu.cn)
†Contributed by ZHAO YaPu (Associate Editor)

models for textured surfaces. For example, the effective slip length l_s can be expressed as:

$$l_s = (L/\pi)\ln\left[\sec(\varphi\pi/2)\right],$$

in which L is the horizontal distance between the roughness peaks and φ was the proportion of actual solid-liquid interface [28–30]. Although the slip length is connected to the surface roughness explicitly, these models do not involve descriptions about the related physical mechanism such as surface wettability or applied shear stress.

More recently, slip models [27,31] based on Frenkel-Eyring molecular kinetic theory (MKT) were designed and sculpted. In the original MKT framework, the liquid flow is treated as a stress-modified molecular rate process. The potential well hypothesis was proposed to describe liquid-solid interactions [32,33]. Further, this concept was developed by Blake et al. [34,35] to describe the nano-droplet wetting and spreading on smooth surfaces. The driving force for the contact line motion is equal to the out-of-balance surface tension force that arises when the capillary equilibrium is disturbed [34,35]. After that, this theoretical approach was used to describe the electro-elasto-capillarity and relevant issues [36–38]. The MKT slip model was also extended to include the critical shear stress, which determines the onset of the slip, and the energy dissipation near the liquid-solid interface with high shear stress [27].

In this work, we applied the extended MKT slip model to textured surfaces, including the chemically textured pattern with alternating stripes of different wettability and the topographically textured pattern with different shapes of grooves. For smooth surfaces, the liquid molecules were assumed to flow unobtrusively with symmetrical potential well periodically. However, it becomes more complicated to give an appropriate account of the potential energy profile for textured surfaces. In this work, through introducing "averaging effect" in the potential well depth of the classic MKT, we advanced the idea of an equivalent depth of potential well and validated it by MD simulations, in which a model with liquid flow confined between two stationary solid walls were simulated. The slip velocity at the solid surface is obtained from the MD simulation and analyzed using the extended MKT slip model. It was assumed that this extended MKT slip model has its prominent advantages. Firstly, with the introduction of the equivalent depth of potential well, this model demonstrates more immediate physical significance for the boundary slip on textured surfaces. Secondly, the analytical expression of this model can be compared with the MD results since it uses parameters consistent with the ones used in the simulations. Thirdly, this slip model can provide more comprehensive understanding of the liquid flow on atomic scale through considering the influence of the solid-liquid interactions and applied shear stress on the nano-flow. Finally, the slip velocity shear-rate dependence can be predicted using this model, since the nonlinear increase of the slip velocity under high shear stress can be approximated by a hyperbolic sine function. The paper is organized as follows. The details of MD simulations are described in sect. 2. The MD simulation results of slip velocity and corresponding MKT analysis on chemically and topographically textured surfaces are presented in sect. 3. The conclusions are given in sect. 4.

2 Models and methods

To investigate the boundary slip behavior and its mechanism on textured surfaces, we consider both chemically and topographically patterned surfaces as shown schematically in Figure 1. The solid walls are parallel to the *xy* plane. The atoms are arranged based on the face-centered cubic crystal structure. As depicted from a side view in Figure 1(a), the chemically textured surfaces are referred to smooth surfaces which are patterned with alternating stripes of different wettability. Various proportions of nonwetting regions, such as 33%, 50% and 67% are used in the simulation, which corresponds to a nonwetting/wetting ratio of 1:2, 1:1 and 2:1, respectively. The topographically textured surfaces are illustrated in Figure 1(b). The surfaces are regularly corrugated and three kinds of groove shapes are used, which are rectangular, positive zigzag and negative zigzag. We may expect that inhomogeneous surfaces or materials would strengthen the interfacial effect [39]. Our study is focusing on the effect of molecular-scale surface corrugation on the slip behavior and the wall configuration of larger scale is not in the scope of our present research [16]. For fluid flows along the *x* axis, positive/negative means that the exterior normal of the inclined plane of each groove has a positive/negative component. The grooved configuration is arranged periodically and every period takes up the same length in the *x*-direction. Furthermore, the depth of the rectangular grooves is equal to the maximum depth of the zig-

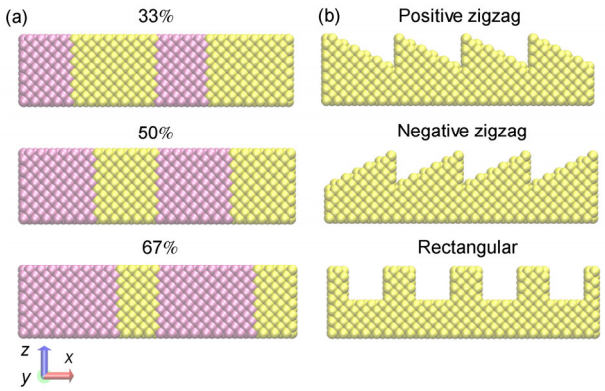

Figure 1 (Color online) Geometries of textured surfaces from front view. (a) Chemically textured surfaces patterned by stripes of different wettabilities. (b) Topographically textured surfaces with positive zigzag, negative zigzag and rectangular shapes from the top to bottom, respectively. Snapshots of the systems are made in VMD [40].

zag ones, which maintain the same groove volume in order to examine the effects of groove shapes on the boundary slip.

The extended simple point charge (SPC/E) model [41] is used to describe the pairwise interactions between any two water molecules. The potential function of the SPC/E model includes two terms, a Lennard-Jones (LJ) term and a Coulombic term. The long-range Coulombic interaction is calculated using a particle-particle particle-mesh (PPPM) [42] solver with an accuracy of 10^{-4}. The interactions between the water molecules and solid walls are described by the LJ interactions:

$$E(r) = 4\varepsilon\left[\left(\frac{\sigma}{r}\right)^{12} - \left(\frac{\sigma}{r}\right)^{6}\right], \quad (1)$$

where ε and σ are the energy and length scales respectively, while r is the distance of separation. Surfaces with different wettabilities are achieved by changing the solid-liquid interaction parameter ε. For liquid-liquid interactions, ε_{ll} = 0.1554 kcal/mol and σ_{ll} = 3.166 Å. For solid-liquid interactions, ε_{ls} is set to be 0.4 or 0.1 kcal/mol in the chemically textured surfaces for the wetting or nonwetting surfaces, respectively. σ_{ls} = 3.0 Å. The cutoff distance for these LJ interactions is set to be 10.0 Å.

All simulations were performed using the LAMMPS package [43]. Periodic boundary conditions were adopted in x- and y-directions, with those of non-periodic in the z-direction. During the calculation of long-range Coulombic interactions, the system is treated to be periodic in z-direction by inserting empty volume between atom slabs and turning off the slab-slab interactions [44]. The size of the simulation box is 10.2 nm × 2.04 nm × 16.0 nm. The simulations were carried out in constant number of molecules, volume, and temperature (NVT) ensemble. The equations of motion were solved using the velocity-Verlet algorithm with a time step of 1.0 fs. After an equilibration run of 100 ps, an additional acceleration along x direction is imposed on every water molecule during the subsequent simulation time to simulate a force driven Poiseuille flow. The shear stress is $\tau = \rho a L_z/2$, where ρ is the liquid density and L_z is the distance between two stationary walls. A standard τ_0 is defined as τ_0 = 20.92 MPa. In our MD simulations, if the applied shear stress is larger than a certain threshold, the liquid flow would be in accelerated motion far away from equilibrium, which results in an unphysical slip behavior. When the fully-developed flow achieved the steady state, simulation data were gathered and analyzed to obtain the density and velocity profiles. The simulation box was divided into many slices along the z-direction with Δz = 0.2 Å in thickness. The velocity and density in each slice were calculated and averaged over a time duration of 1.0 ns. The two-dimensional velocity and density profiles were obtained by meshing the simulation box into a square grid (0.2 Å × 0.2 Å) in the xz plane.

During the simulations, the system temperature was kept at 300 K using the Nose-Hoover thermostat. It should be noted that the thermostat was applied only along the y- and z-directions to avoid a bias in the flow direction. The wall atoms are fixed rigidly at the lattice sites, thus the interactions among solid atoms can be neglected. It has been argued for a long time that the choice of the thermostating method affects the results [45–50]. After substantial simulations using different thermostats, we found that our main conclusion on the nonlinear increase of the slip velocity with the applied shear stress holds valid. We tried flexible walls with solid atoms tethered to the lattice site via a harmonic spring where only wall atoms are subjected to the thermostat. Our MD results also indicate that the numerical values of the slip velocity are dependent on the spring constant we set in the simulations [16]. Besides, this thermostating method may result in an improper viscous heating accumulation in the fluid [50]. The underlying relationships among the flow behavior, the chosen spring constant and the heat conduction at the interface deserves further investigations, which are beyond the scope of the present work.

3 Results and discussion

3.1 Extended MKT slip model for textured surfaces

The liquid molecules in the vicinity of atomically smooth surface are supposed to be located in a periodically symmetrical potential well with a depth of E_0. Thus, a liquid molecule has to go through the potential well when flowing past a solid surface. Once the shear stress is imposed, the potential energy surface inclined according. The frequency that the molecule hops forward and backward is no longer the same, which results in a net frequency along the direction of external force. The detailed derivation process and introduction about the MKT theory can be found in ref. [7]. The slip velocity is proportional to the exponentiation of the potential well depth E_0 and the hyperbolic sine of the exerted shear stress τ on the liquid molecules, which has a form of

$$V_s = V_0 \exp\left(-\frac{E_0}{k_B T}\right)\sinh\left(\frac{\tau S \lambda}{2k_B T}\right), \quad (2)$$

where $V_0 = 2\lambda k_B T/h$, k_B is the Boltzmann constant, T is the absolute temperature, and h is the Planck constant. S is the effective area per molecule along the flowing direction. λ is the equilibrium separation between liquid molecules. The above-mentioned velocity from Eyring's MKT has also been adopted to explain the mechanism of precursor chain's propagation in a hydrophilic interior corner [51].

The number of water molecules in the first fluid layer (N) next to the solid surface can be calculated during the simu-

lations, with which we can get the effective area per molecule S. λ then can be obtained using $\lambda = \sqrt{S}$. Among all the parameters, the applied shear stress and the depth of potential well are two dominant factors for determining the slip velocity. The potential well depth is determined by the solid-liquid interaction. For the chemically textured surfaces, different wettability is achieved by adopting different solid-liquid interaction parameters. Consequently, the depth of the potential well would change periodically, as shown in Figure 2(a). For the topographically textured surfaces, different groove shapes also exert influence on the solid-liquid interactions. The closer the water molecules to the solid surface, the larger are the solid-liquid interactions. When the water molecules filled up the empty grooves in the Wenzel state, the water molecules in the grooves can be regarded as a whole which exert liquid-liquid interactions on the water molecules in the first layer. However, the liquid-liquid interaction is smaller compared with the solid-liquid interaction in the wetting case. Consequently, for the water molecules in the first layer just above the grooves, the global shape of potential well depth is an average of these liquid-liquid and solid-liquid interactions, which can also be seen in Figure 2(b)–(d). What makes the difference is that the specific value of the potential well depth and the depth gap between the adjacent potential well is smaller compared with that in the Cassie state. For the rectangular, positive zigzag and negative zigzag grooves, the corresponding potential landscapes along the flow direction are illustrated in Figure 2(b)–(d). The shape of the potential well is more complicated than the shape of the corrugations. However, the potential landscape generally reflects the shape of the corrugations.

In the Frenkel-Eyring MKT model, E_0 denotes the activation energy for the molecular displacements [32,33]. When considering the boundary slip on the textured surfaces, we found it is the crucial factor to cover the complex of modeling solid surfaces. The change of the potential well depth implies that the velocity required for a liquid molecule to pass over each energy barrier is different. The slip velocity should be the averaged result of these diverse velocities over the entire potential well. A concept of equivalent depth of potential well is needed to describe the periodical change of the potential well, which is denoted by E_e. E_e should be determined by averaging local intermolecular interactions according to the effect of the surface wettability and geometry. If we replace E_0 in eq. (2) with this E_e, the classical MKT model thus can be used to give a description of the boundary slip on the textured surfaces. We assume that the simplification on E_e gives a concise and reasonable description of the slip behavior on the textured surfaces, in spite of some missing details. Compared with λ or S, a small change in E_e would lead to a significantly larger variation of the slip velocity, especially for wetting surfaces, which means that E_e is the dominant factor in the slip velocity expression. Thus in the following discussions, we leave

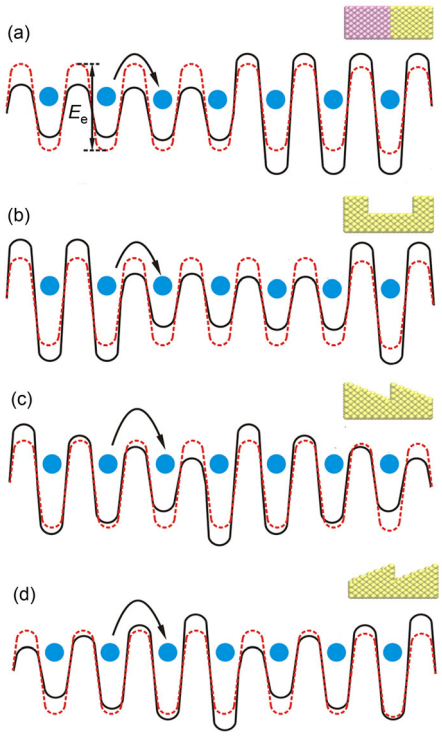

Figure 2 (Color online) Schematic of the potential well for chemically (a) and topographically (b)–(d) textured surfaces (solid lines). The water molecule is denoted by circles. The dash lines represent the equivalent potential well. The depth is represented by E_e. The black arrow indicates the direction that the water molecule jumps from one equilibrium position to the next. The schematic depiction doesn't refer to the actual potential well depth in different configurations. The potential well depth values in the wetting and nonwetting cases were discussed specifically afterwards.

λ and S as constant. This simplification can make the slip velocity expression more concise. Moreover, since the variation of the effective area per particle has been taken into account in the simulations, this effect is included into E_e, which is obtained by fitting our MD results.

3.2 Slip behavior on chemically patterned surfaces

Here let β denote the proportion of nonwetting regions in the total length of the chemically patterned surface. β = 33.3%, 50%, 67.7% were used in the MD simulations. During the simulation, various driving forces were imposed on the liquid confined between the two stationary solid walls.

Figure 3 shows the density profile in the vicinity of the chemically textured surfaces with a shear stress of $1.25\,\tau_0$. In our simulations, if we take $\rho = 10^3$ kg/m^3, v = 500 m/s, $d = 10^{-8}$ m, $\eta = 10^{-3}$ Pa s, the Reynolds number $Re = \rho v d/\eta$ can be estimated to be less than 10, which indicates that the flows is still in the laminar regimes. As concerns the flow near a solid wall, the fluid in the vicinity of the solid show different properties from their bulk counterparts [52–55]. In our work, the density stratification can be observed along the vertical (z) direction. In the horizontal (x) direction, the

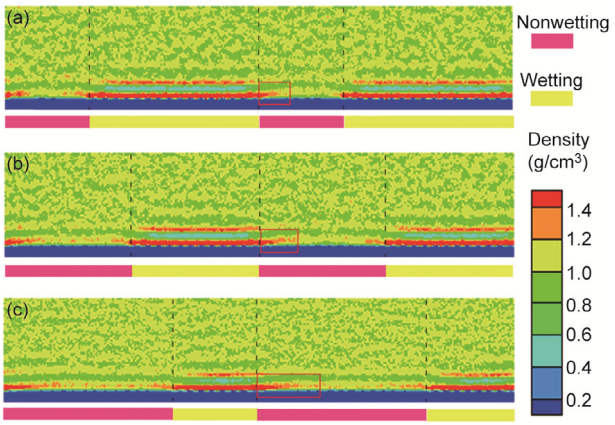

Figure 3 Density profiles of liquid on the chemically textured surfaces with an acceleration of $1.25\,\tau_0$. The black dash lines divide the wetting and nonwetting regions. The color stripes under the density profiles correspond to the wetting (yellow) and nonwetting (mauve) regions in the chemically textured surfaces. The density profiles of $\beta = 33.3\%$ (a), 50% (b), 67.7% (c) are illustrated from the top to the bottom. The advancing trend of density is indicated in the red box.

periodical changes of the density correspond to the variations of the surface wettability. Stronger layering structures appear in the vicinity of the wetting region due to a larger solid-liquid interaction. The dash lines in Figure 3 divide the flow field according to the width of the wetting and nonwetting regions. On the first liquid layer adsorbed near the wetting region, one can find that this liquid layer exhibits obvious advancing trend into the nonwetting region along the flow direction with the increasing of β, which is denoted by the red box in Figure 3. With the increasing proportion of the nonwetting regions, it is getting more difficult for the solid surface to adsorb and immobilize the water molecules. As a result, the advancing trend of the maximum density due to the inertia effect becomes more obvious.

To illustrate the effect of the nonwetting and wetting surfaces modeled in the simulations, we studied the spreading of a water nanodroplet on these surfaces with the same liquid-solid interaction parameters. The contact angle of the nanodroplet is 135° and 61° for the nonwetting and wetting cases, respectively. It should be noted that the solid-liquid interactions are closely connected to the contact angle, especially for the homogeneous surfaces. A quasi-universal relationship between the slip length and the static contact angle was established [20]; while another literature indicates that contact angles larger than 90° do not necessarily to attain hydrodynamic slip [26]. Instead, it was demonstrated that slip is determined by the interfacial water molecule distribution and the strength of liquid-solid interactions [26]. In our work, the contact angle was provided only to give an intuitive impression of the different LJ parameters used in the MD simulations.

The MD results of the slip velocity as a function of shear stress τ are plotted in Figure 4. Despite the slip velocity is on the order of 100 m/s, the laminar flow can still be guaranteed. In addition, the thermal velocity in MD simulations under 300 K is usually on the order of 100 m/s. Thus large flow/slip velocities are feasible so that the fluid velocity profile could be retrieved with reasonable accuracy with minimal fluctuations in the velocity profile due to thermal noise [56]. One can find that, under the same shear stress, the slip velocity is smaller for a smaller proportion of the nonwetting regions. This is because the wetting regions correspond to stronger liquid-solid interactions. In Figure 4, the MD results of the slip velocity can be fitted with the extended MKT slip model for the textured surfaces. Different values of the equivalent depth of potential well are used for different β. The MKT slip model is in good agreement with the MD results.

To simplify the description of E_e, define $E_s = k_B T$. Consider two limiting cases with $\beta = 0\%$ and $\beta = 100\%$. The MKT fitting results show that the depth of potential well is $E_w = 8.5E_s$ and $E_n = 3.3E_s$ respectively for the wetting and nonwetting cases. For the chemically textured surfaces, larger slip velocity corresponds to smaller equivalent depth of the potential well, which suggests that the equivalent depth of the potential well decreases with increasing β. Based on the concept of the equivalent depth of potential well and comparison of its values in different situations, one finds that E_e can be approximately calculated as:

$$E_e = \beta E_n + (1-\beta) E_w, \tag{3}$$

For the equivalent depth of the potential well of the chemically textured surfaces with different β, E_e is a linear combination of E_w and E_n. MD simulations were conducted to verify the theoretical hypothesis expressed in eq. (3). The MKT fitted results of E_e, the theoretical value acquired ac-

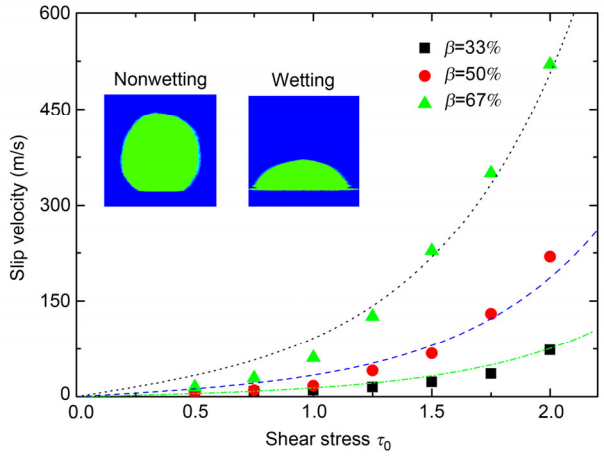

Figure 4 MD results and MKT fitting of slip velocity on chemically patterned surfaces. The slip velocity increases with the increasing proportions of the nonwetting region. The MKT analysis turns out to correspond with the MD results. The two insets display the density profiles of a water nanodroplet wetting on the nonwetting and wetting surfaces and the contact angle is 135° and 61°, respectively.

cording to eq. (3) and relative error are summarized in Table 1. The equivalent depth of the potential well can be used to describe the boundary slip on the chemically textured surfaces and its value can be estimated as the linear combination of E_n and E_w.

For striped surface with large slip, an "inverse law" is proposed at heterogeneous surfaces with alternative stripes of infinite-slip and partial-slip boundary conditions, which is written as $1/B_0 = \varsigma/b_0 + (1-\varsigma)/b_1$ [57]. This quantitative relation is acquired through averaging of the friction. We think that eq. (3) comes out with a similar idea with the "inverse law", using the average of the activation energy instead of that of the friction.

3.3 Slip behavior on topographically textured surfaces

For the topographically textured surfaces, both the wetting and nonwetting cases were investigated. The solid-liquid interactions for the wetting and nonwetting cases in the topographically textured surfaces are chosen as 0.3 kcal/mol and 0.2 kcal/mol, respectively. The reason to do this adjustment is that the distribution of the water molecules is closely related to the solid-liquid interactions owing to the grooves. If ε_{ls} is set to be 0.1 kcal/mol in the topographically textured surfaces, no water molecules will enter the grooves and a large slip velocity will be rendered at a small shear stress. Moreover, we know from our simulation results that once the solid-liquid interaction parameter exceeds 0.3 kcal/mol, all the grooves are filled up completely. So we have made a justifiable adjustment for the solid-liquid interactions. The MD simulations on the boundary slip were first performed for the nonwetting case. The MD results of the slip velocity as a function of shear stress τ are plotted in Figure 5. The slip velocity as calculated from the extended MKT slip model for the textured surfaces shows that the equivalent depth of potential well for the rectangular, positive zigzag and negative zigzag grooves are $4.0E_s$, $6.8E_s$ and $6.2E_s$, respectively. The fitting based on the MKT slip model is in accordance with the MD results. These results suggest that the surface nanostructures have a significant influence on the boundary slip behavior.

Before applying shear stress, water molecules are confined between the textured surfaces with empty grooves. Then the system achieves the steady state under the action of the shear stress. For the model with rectangular grooves at $\tau = 4\tau_0$ and $5\tau_0$, the shear stress is so large that the liquid flow cannot maintain a steady state. In other words, the flow response is no longer linear. The MD snapshots are shown in the insets of Figure 5. The grooves of the positive zigzag structure are completely filled with water molecules, which is known as the Wenzel state [58]. The Cassie state [59] appears in the rectangular grooves, as the liquid molecules do not enter the grooves. While for the negative zigzag structure, the grooves are partly filled up, corresponding to an intermediate state between the Cassie and Wenzel states. As discussed in the previous discussion, the farther are the water molecules from the solid surfaces, the smaller is the solid-liquid interaction. Different liquid distributions in the grooves result in different interactions between the water molecules and the textured surface, which leads to the difference of the slip velocities even for the same shear stress. Moreover, comparing the geometry of the two kinds of zigzag surfaces, the vertical plane on the right side of each groove in the positive zigzag structure introduces the obstruction effect on the motion of water molecules, while the vertical plane on the left side of each groove in negative zigzag structure has limited influence on the liquid flow. Based on the MD simulation results, one can propose that there are two mechanisms for the slip behavior on the topographically textured surfaces, which are the liquid distribution due to surface wettability and the obstruction effect of nanostructures. For the same shear stress, the slip velocity on the positive zigzag surface is smaller than that on the negative zigzag surface. The slip velocity on the rectangular surface is larger due to the weak liquid-solid interactions without any obstruction effect on the liquid flow.

Figure 6 shows the MD simulations on the topographically textured surfaces with wetting surface. Based on the extended MKT slip model, the equivalent depth of the potential well is found to be $7.0E_s$, $7.0E_s$ and $6.8E_s$ for the rectangular, positive zigzag and negative zigzag structures, respectively. One can also find that for the shear stress smaller than $4\tau_0$, the slip velocities are almost the same for

Table 1 Comparisons between the MKT fitted E_e and the theoretical value acquired from eq. (3)

β	MKT fitted E_e	E_e from eq. (3)	Error (%)
33%	$7.0E_s$	$6.8\ E_s$	2.8
50%	$6.0\ E_s$	$5.9\ E_s$	1.7
67%	$5.0\ E_s$	$5.0\ E_s$	0

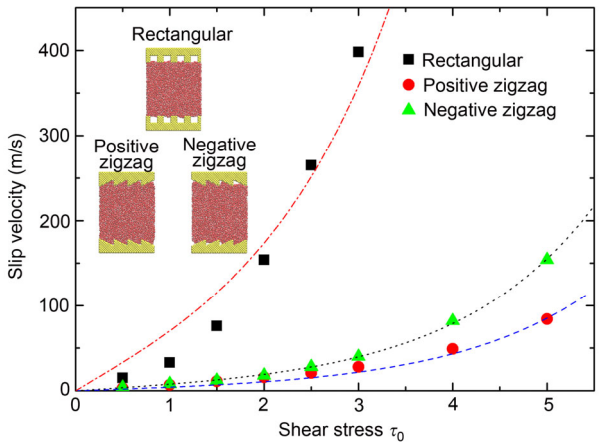

Figure 5 (Color online) MD results of the slip velocity as a function of shear stress in the nonwetting case. The velocities were fitted with eq. (2). The insets show the MD snapshots of three configurations. The fitted velocity curve of the rectangular model was denoted by the dash dot lines, while the slip velocities of the positive zigzag model and the negative zigzag model were fitted using dash line and dot line, respectively.

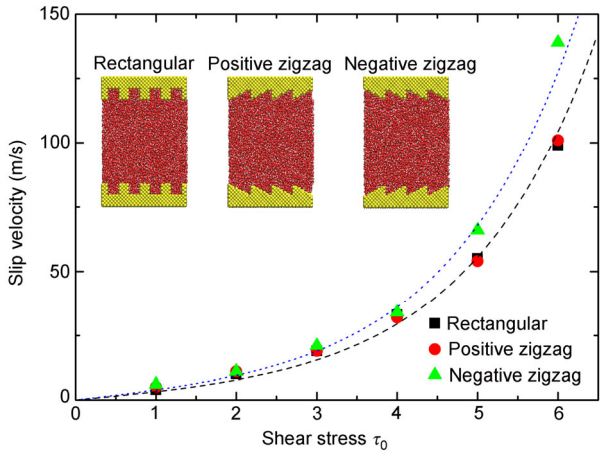

Figure 6 MD results of the slip velocity as a function of shear stress for the wetting surfaces. The velocities were fitted with the extended MKT slip model. The insets show the MD snapshots of the three configurations, in which the grooves were fully filled with water molecules. The fitted velocity curve of the negative zigzag model was denoted by the dot lines. The slip velocities of the positive zigzag model and the rectangular model were almost the same and were fitted using the same dash line.

the rectangular, positive zigzag and negative zigzag surfaces. For larger shear stress, the slip velocity on the negative zigzag surface is larger than that on the other two kinds of textured surfaces. Due to the large solid-liquid interactions, all the grooves are filled up with water molecules in these wetting surfaces, which can be observed in the insets of Figure 6. Since the water molecules fully filled the grooves, the obstruction effect of nanostructure on the liquid flow should be taken into account for higher shear stress.

Comparing the data presented in Figures 5 and 6 (only the LJ parameter ε which characterizes the solid-liquid interactions was changed), we obtain some interesting observations. (1) Despite wetting or nonwetting surfaces, the equivalent depth of potential well for positive zigzag surface does not change too much. This indicates that for the positive zigzag corrugations, the obstruction effect of nanostructures dominates the boundary slip behaviors, rather than the surface wettability. (2) The slip velocity plots for rectangular and positive zigzag geometries collapse into one in Figure 6. According to the variation of E_e in our extended MKT slip model, we should consider the effect of some concrete aspects related to the textured surfaces, such as the interfacial water molecule distribution and the strength of water-solid interactions. As water-solid interactions increases, the water molecules start to fill the rectangular grooves, which means that the distribution of water molecules at contact with the solid is changed. The obstruction effect of nanostructures on the liquid flow should be taken into account for the cases of rectangular grooves where the corresponding slip velocity was suppressed significantly. Consequently, the collapse happens for liquid-solid interactions beyond a critical threshold for wetting.

Based on the above analysis, the distribution of water molecules at contact with the solid, which is affected by the water-solid interactions, is the origin of the aforementioned obstruction effect of nanostructures. The vertical plane on the right side of each groove in the rectangular and positive zigzag structures blocks on the liquid flow under shear. One can infer that the obstruction effect is more obvious for larger shear stress. For the negative zigzag structure, the vertical plane on the left side of the groove has no significant influence on the liquid flow in the x-direction. To provide direct insight into the second mechanism about the obstruction effect, the velocity and density profiles in the vicinity of the zigzag textured surfaces are shown in Figure 7. The red arrows at the bottom indicate the flow direction. As one can find from the velocity profiles illustrated in Figures 7(a) and (b), the velocity contour titles down in the negative zigzag groove, while it travels up in the positive zigzag groove. In order to demonstrate the velocity varia-

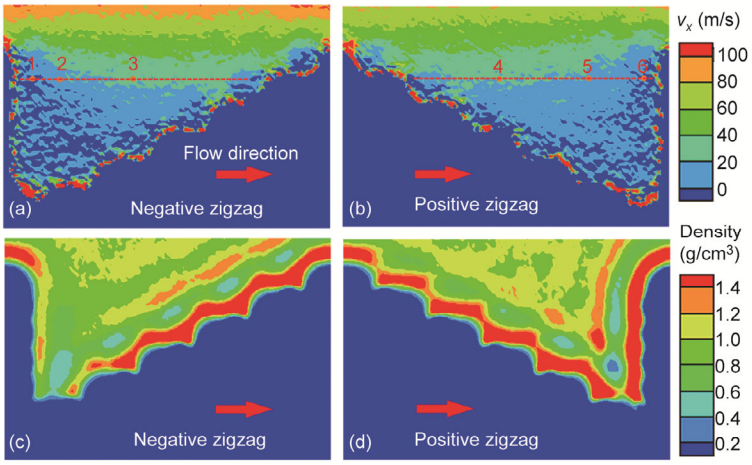

Figure 7 Velocity and density profiles in the vicinity of the zigzag textured surfaces for the wetting surface with the shear stress of $5\tau_0$. The red arrows at the bottom indicate the flow direction. The selected points on the dotted line in (a) and (b) can clearly demonstrate the velocity variation due to the obstruction effect of the zigzag grooves.

tion in each groove, we have added a dotted line for fixed z in Figures 7(a) and (b), on which three points are selected, respectively. The flow velocity increases along the flow direction in a single unit of the negative zigzag groove. On the contrary, the velocity near the positive zigzag surface decreases due to the blocking by the vertical plane of the groove. From the density profiles shown in Figures 7(c) and (d), one can find that the liquid density is large near the vertical plane of the positive zigzag groove. This provides the evidence of the obstruction effect of the positive zigzag grooves, which corresponds to the difference of the slip velocities for the topographically textured surfaces shown in Figure 6.

4 Conclusion

In summary, we proposed a theoretical model for the boundary slip on textured surfaces based on the Frenkel-Eyring molecular kinetic theory. The equivalent depth of potential well was introduced to characterize the effect of surface wettability and nano-corrugations. This extended MKT slip model can predict the nonlinear increase of the slip velocity under high shear stress on textured surface. MD simulations were carried out to study the boundary slip on both chemically and topographically textured surfaces, and the results were in good agreement with the MKT slip model. For the chemically textured surfaces, the equivalent depth of potential well is a linear combination of the potential well depths for the nonwetting and wetting smooth surfaces. According to an intuitive comparison of E_e due to different corrugations, we found that the liquid distribution near the grooves and the obstruction effect of the nanostructures are two possible mechanisms that influence the topographically textured surface on the boundary slip at the molecular level. With the applications of the extended MKT slip model, this work provides a microscopic interpretation about the influence of the surface corrugation on the interfacial flow, and extends our understanding of the boundary slip mechanism on textured surfaces.

This work was supported by the National Natural Science Foundation of China (Grant Nos. U1262103, 11302218 and 11172289), Anhui Provincial Natural Science Foundation (Grant Nos. 1308085QA10 and 1408085J08) and the Fundamental Research Funds for the Central Universities of China.

1 Gogte S, Vorobieff P, Truesdell R, et al. Effective slip on textured superhydrophobic surfaces. Phys Fluids, 2005, 17: 051701
2 Barthlott W, Neinhuis C. Purity of sacred lotus, or escape from contamination in biological surfaces. Planta, 1997, 202: 1–8
3 Frohnapfel B, Jovanović J, Delgado A. Experimental investigations of turbulent drag reduction by surface-embedded grooves. J Fluid Mech, 2007, 590: 107–116
4 Bechert D W, Bruse M, Hage W, et al. Experiments on drag-reducing surfaces and their optimization with an adjustable geometry. J Fluid Mech, 1997, 338: 59–87
5 Tu Y S, Xiu P, Wan R Z, et al. Water-mediated signal multiplication with y-shaped carbon nanotubes. Proc Natl Acad Sci USA, 2009, 106: 18120–18124
6 Xiu P, Zhou B, Qi W P, et al. Manipulating biomolecules with aqueous liquids confined within single-walled nanotubes. J Am Chem Soc, 2009, 131: 2840–2845
7 Zhao Y P. Physical Mechanics of Surfaces and Interfaces. Beijing: Science Press, 2012
8 Zhao Y P. Moving contact line problem: Advances and perspectives. Theor Appl Mech Lett, 2014, 4: 034002
9 Neto C, Evans D R, Bonaccurso E, et al. Boundary slip in newtonian liquids: A review of experimental studies. Rep Prog Phys, 2005, 68: 2859–2897
10 Truesdell R, Mammoli A, Vorobieff P, et al. Drag reduction on a patterned superhydrophobic surface. Phys Rev Lett, 2006, 97: 044504
11 Mongruel A, Chastel T, Asmolov E S, et al. Effective hydrodynamic boundary conditions for microtextured surfaces. Phys Rev E, 2013, 87: 011002
12 Yuan Q Z, Zhao Y P. Multiscale dynamic wetting of a droplet on a lyophilic pillar-arrayed surface. J Fluid Mech, 2013, 716: 171–188
13 Wu C M, Lei S L, Qian T Z, et al. Stick-slip motion of moving contact line on chemically patterned surfaces. Commun Comput Phys, 2010, 7: 403–422
14 Capozza R, Fasolino A, Ferrario M, et al. Lubricated friction on nanopatterned surfaces via molecular dynamics simulations. Phys Rev B, 2008, 77: 235432
15 Priezjev N V, Darhuber A A, Troian S M. Slip behavior in liquid films on surfaces of patterned wettability: Comparison between continuum and molecular dynamics simulations. Phys Rev E, 2005, 71: 041608
16 Priezjev N V. Effect of surface roughness on rate-dependent slip in simple fluids. J Chem Phys, 2007, 127: 144708
17 Priezjev N V. Molecular diffusion and slip boundary conditions at smooth surfaces with periodic and random nanoscale textures. J Chem Phys, 2011, 135: 204704
18 Tretyakov N, Müller M. Correlation between surface topography and slippage: A molecular dynamics study. Soft Matter, 2013, 9: 3613–3623
19 Wang X P, Qian T Z, Sheng P. Moving contact line on chemically patterned surfaces. J Fluid Mech, 2008, 605: 59–78
20 Huang D M, Sendner C, Horinek D, et al. Water slippage versus contact angle: A quasiuniversal relationship. Phys Rev Lett, 2008, 101: 226101
21 Patankar N A. On the modeling of hydrophobic contact angles on rough surfaces. Langmuir, 2003, 19: 1249–1253
22 Thompson P A, Troian S M. A general boundary condition for liquid flow at solid surfaces. Nature, 1997, 389: 360–362
23 Ma M D, Shen L M, Sheridan J, et al. Friction of water slipping in carbon nanotubes. Phys Rev E, 2011, 83: 036316
24 Vinogradova O I. Drainage of a thin liquid film confined between hydrophobic surfaces. Langmuir, 1995, 11: 2213–2220
25 Wei N, Peng X S, Xu Z P. Breakdown of fast water transport in graphene oxides. Phys Rev E, 2014, 89: 012113
26 Ho T A, Papavassiliou D V, Lee L L, et al. Liquid water can slip on a hydrophilic surface. Proc Natl Acad Sci USA, 2011, 108: 16170–16175
27 Wang F C, Zhao Y P. Slip boundary conditions based on molecular kinetic theory: The critical shear stress and the energy dissipation at the liquid-solid interface. Soft Matter, 2011, 7: 8628–8634
28 Philip J R. Flows satisfying mixed no-slip and no-shear conditions. Z Angew Math Phys, 1972, 23: 353–372
29 Philip J R. Integral properties of flows satisfying mixed no-slip and no-shear conditions. Z Angew Math Phys, 1972, 23: 960–968
30 Lauga E, Stone H A. Effective slip in pressure-driven stokes flow. J Fluid Mech, 2003, 489: 55–77
31 Yang F Q. Slip boundary condition for viscous flow over solid surfaces. Chem Eng Comm, 2010, 197: 544–550
32 Frenkel J I. Kinetic Theory of Liquids. Oxford: Oxford University

Press, 1946
33 Glasstone S, Laidler K J, Eyring H. The Theory of Rate Processes. New York: McGraw-Hill, 1941
34 Blake T D, Haynes J M. Kinetics of liquid/liquid displacement. J Colloid Interface Sci, 1969, 30: 421–423
35 Blake T D. The physics of moving wetting lines. J Colloid Interface Sci, 2006, 299: 1–13
36 Yuan Q Z, Zhao Y P. Precursor film in dynamic wetting, electrowetting, and electro-elasto-capillarity. Phys Rev Lett, 2010, 104: 246101
37 Zhu X Y, Yuan Q Z, Zhao Y P. Capillary wave propagation during the delamination of graphene by the precursor films in electro-elasto-capillarity. Sci Rep, 2012, 2: 927
38 Wang F C, Zhao Y P. Contact angle hysteresis at the nanoscale: A molecular dynamics simulation study. Colloid Polym Sci, 2013, 291: 307–315
39 Yang F Q. Diffusion-induced stress in inhomogeneous materials: concentration-dependent elastic modulus. Sci China-Phys Mech Astron, 2012, 55(6): 955–962
40 Humphrey W, Dalke A, Schulten K. VMD: Visual molecular dynamics. J Mol Graphics, 1996, 14: 33–38
41 Berendsen H J C, Grigera J R, Straatsma T P. The missing term in effective pair potentials. J Phys Chem, 1987, 91: 6269–6271
42 Hockney R W, Eastwood J W. Computer Simulation Using Particles. New York: Adam Hilger, 1988
43 Plimpton S. Fast parallel algorithms for short-range molecular dynamics. J Comput Phys, 1995, 117: 1–19
44 Yeh I C, Berkowitz M L. Ewald summation for systems with slab geometry. J Chem Phys, 1999, 111: 3155–3162
45 Martini A, Hsu H Y, Panankar N A, et al. Slip at high shear rates. Phys Rev Lett, 2008, 100: 206001
46 McBride S P, Law B M. Viscosity-dependent liquid slip at molecularly smooth hydrophobic surfaces. Phys Rev E, 2009, 80: 060601
47 Kannam S K, Todd B D, Hansen J S, et al. Slip length of water on graphene: Limitations of non-equilibrium molecular dynamics simulations. J Chem Phys, 2012, 136: 024705
48 Lichter S, Roxin A, Mandre S. Mechanisms for liquid slip at solid surfaces. Phys Rev Lett, 2004, 93: 086001
49 Yong X, Zhang L T. Thermostats and thermostat strategies for molecular dynamics simulations of nanofluidics. J Chem Phys, 2013, 138: 084503
50 Yong X, Zhang L T. Slip in nanoscale shear flow: Mechanisms of interfacial friction. Microfluid Nanofluid, 2013, 14: 299–308
51 Yuan Q Z, Zhao Y P. Topology-dominated dynamic wetting of the precursor chain in a hydrophilic interior corner. Proc R Soc A, 2012, 468: 310–322
52 Sun Z W, Xu S H. Two examples of using physical mechanics approach to evaluate colloidal stability. Sci China-Phys Mech Astron, 2012, 55(6): 933–939
53 Yu Y, Wu Q, Zhang K, et al. Effect of triple-phase contact line on contact angle hysteresis. Sci China-Phys Mech Astron, 2012, 55(6): 1045–1050
54 Wang X W, Yu Y. Analysis of the shape of heavy droplets on flat and spherical surface. Sci China-Phys Mech Astron, 2012, 55(6): 1118–1124
55 Zhang W L, Qian J, Yao H M, et al. Effects of functionally graded materials on dynamics of molecular bond clusters. Sci China-Phys Mech Astron, 2012, 55(6): 980–988
56 Joseph S, Aluru N R. Why are carbon nanotubes fast transporters of water? Nano Lett, 2008, 8: 452–458
57 Cottin-Bizonne C, Barentin C, Charlaix E, et al. Dynamics of simple liquids at heterogeneous surfaces: Molecular-dynamics simulations and hydrodynamic description. Eur Phys J E, 2004, 15: 427–438
58 Wenzel R N. Resistance of solid surfaces to wetting by water. Ind Eng Chem, 1936, 28: 988–994
59 Cassie A B D, Baxter S. Wettability of porous surfaces. Trans Faraday Soc, 1944, 40: 546–551